595

High-velocity impact of large caliber tungsten projectiles on ordinary Portland and calcium aluminate cement based HPSFRC and SIFCON slabs. Part I: experimental investigations

H. Korucu*[1] and P. Gülkan[2a]

[1]Turkish Naval Forces Command, 06100 Bakanlıklar, Ankara, Turkey
[2]Department of Civil Engineering, Cankaya University, 06810 Ankara, Turkey

Abstract. Impact experiments have been carried out on concrete slabs. The first group was traditionally manufactured, densely reinforced concrete targets, and the next were ordinary Portland and calcium aluminate cement based HPSFRC (High performance steel fiber reinforced concrete) and SIFCON (Slurry infiltrated concrete) targets. All specimens were hit by anti-armor tungsten projectiles at a muzzle velocity of over 4 Mach causing destructive perforation. In Part I of this article, production and experimental procedures are described. The first group of specimens were ordinary CEM I 42.5 R cement based targets including only dense reinforcement. In the second and third groups, specimens were produced using CEM I 42.5 R cement and Calcium Aluminate Cement (CAC40) with ordinary reinforcement and steel fibers 2 percent in volume. In the fourth group, SIFCON specimens including 12 percent of steel fibers without reinforcement were tested. A high-speed camera was used to capture impact and residual velocities of the projectile. Sample tests were performed to obtain mechanical properties of the materials. In the companion Part II of this study, numerical investigations and simulations performed will be presented. Few studies exist that examine high-velocity impact effects on CAC40 based HPSFRC targets, so this investigation gives an insight for comparison of their behavior with Portland cement based and SIFCON specimens.

Keywords: high-velocity impact; projectile; calcium aluminate cement; steel fibers; reinforced concrete; SIFCON

1. Introduction

The impinging of very high velocity projectiles on conventional concrete targets is a current problem in impact engineering and has security implications. The study of the behavior of reinforced concrete targets under projectile impact is important for the design of protective structures widely used in military and strategic civil structures. To date the problem has been investigated both experimentally and analytically but the number of studies on high-velocity (> 1000 m/s) projectile impacting reinforced concrete has remained limited.

---

*Corresponding author, Ph.D., E-mail: korucu_h@yahoo.com
[a]Ph.D., E-mail: polatgulkan@cankaya.edu.tr

Dancygier (2009) reported experiments that used projectiles weighing 1.5 kg, while most other studies were performed by using lighter ammunition. Teng *et al.* (2008) performed experiments using 45 g projectiles with a velocity of 2474 m/s impacting steel fiber reinforced concrete. Vassoughi *et al.* (2007) and Quek *et al.* (2010) also carried out impact experiments with 34 g and 17 g projectiles, respectively, with velocities of 700 m/s and 600 m/s, striking concrete specimens. Zhang *et al.* (2005) reported tests including 12.6 mm ogive-shaped nose projectiles with a velocity of 700 m/s and concrete of 45-235 MPa compressive strength. Luo *et al.* (2000) and Beppu *et al.* (2008) have performed impact tests at lower velocities on cement based composites.

Other investigators have performed high-velocity impact experiments using targets composed of materials other than concrete. Puente *et al.* (2009) carried out experiments and did their numerical validation using steel projectiles of 1.1 g impacting on carbon/epoxy laminates with a velocity of 600 m/s. Zhang *et al.* (2009) carried out experiments with aluminum beams and 4.3 g of projectiles at 772 m/s velocity. Impact experiments of Özşahin *et al.* (2010) consisted of AA 6061 T651 aluminum plates coated with plasma spray and 8 g bullets with a velocity of 380 m/s. Orphal *et al.* (1997) presented results from a series of experiments with bullets fired into thick confined boron carbide targets, with a velocity range between 1500-4651 m/s.

In the context of this study, high-velocity impact tests on four groups of specimens have been performed. In the first group, four conventional densely reinforced concrete targets were tested. In the second group, three specimens that consisted of dense reinforcement in the same configuration with the first group and 2 percent of steel fibers by volume were tested. These three specimens were manufactured using CEM I 42.5 R cement while the third group of specimens were produced with CAC40 (Calcium Aluminate Cement). Material proportions and configurations of the third group specimens were the same as the second group. In the fourth group, SIFCON (Slurry Infiltrated Fiber Concrete) specimens consisting of 12 percent in volume of steel fibers with no reinforcement were tested. The slurry was CEM I 42.5 R based. The target specimens were 2×2 m slabs, with either 0.4 or 0.6 m thickness. Large-caliber tungsten projectiles 105 mm in diameter and 1485 m/s initial velocity were used. The core mass of the projectile was 5.57 kg. The tests were recorded using high-speed cameras to obtain impact and exit velocity and perforation. Various material tests were done to define the material characteristics for use in the computational software.

In this part, only the experimental procedure will be described. It is intended here to investigate the local impact effects caused by high-velocity impact on concrete specimens that have various material specifications and configurations of large-caliber projectiles with a velocity above 4 Mach and a weight of 5.57 kg. Effects of these various materials in affecting residual velocity and dictating crater formation were observed. It is very exceptional to have high-velocity impact effects on CAC40 based HPSFRC targets reported in free-access literature, so an opportunity to compare their behavior with Portland cement based and SIFCON specimens is enabled.

2. Experimental procedure

The experimental program was carried out in two areas: sample tests were made in the laboratory for determination of the basic conventional mechanical properties of the materials used in specimens, and high-velocity impact tests on slabs were carried out in a military firing range. Descriptions of the physical specifications of the specimens are given in Table 1 where specimens are designated with their experimental group number and sequence number.

Table 1 Specifications of specimens

No.	Dimensions			Cement Type	Reinforcement configuration (Flexural – Confinement)* (mm)	Fiber Ratio (percent)
	Length (m)	Width (m)	Thickness (m)			
1-1	2.00	2.00	0.60	CEM I 42.5 R	17 ϕ 22 - ϕ10/15	---
1-2	2.00	2.00	0.60	CEM I 42.5 R	17 ϕ 22 - ϕ10/20	---
1-3	2.00	2.00	0.40	CEM I 42.5 R	17 ϕ 18 - ϕ10/20	---
1-4	2.00	2.00	0.40	CEM I 42.5 R	17 ϕ 18 - ϕ10/15	---
2-1	2.00	2.00	0.60	CEM I 42.5 R	17 ϕ 22 - ϕ10/20	2
2-2	2.00	2.00	0.60	CEM I 42.5 R	17 ϕ 22 - ϕ10/20	2
2-3	2.00	2.00	0.60	CEM I 42.5 R	17 ϕ 22 - ϕ10/20	2
3-1	2.00	2.00	0.60	CAC40	17 ϕ 22 - ϕ10/20	2
3-2	2.00	2.00	0.60	CAC40	17 ϕ 22 - ϕ10/20	2
3-3	2.00	2.00	0.60	CAC40	17 ϕ 22 - ϕ10/20	2
4-1	2.00	2.00	0.60	CEM I 42.5 R	---	12
4-2	2.00	2.00	0.60	CEM I 42.5 R	---	12
4-3	2.00	2.00	0.60	CEM I 42.5 R	---	12

*See Fig. 2.

2.1 Materials and proportioning

In the first group, two types of concrete with 30 MPa and 55 MPa compressive strength were designed using Portland cement and crushed limestone with maximum size of 16-22.4 mm. Normal and hyper plasticizers were added to obtain a better workability of the mortar.

Two types of concrete were used in the second and third groups: 61 MPa with CEM I 42.5 R and 87 MPa of CAC40 based. The hyper plasticizer Glenium 51 was used for CEM I 42.5 R and CAC40 to obtain an improved workability of the concrete mortar.

In the fourth group, the compressive strength of the SIFCON was 58 MPa and super plasticizer Rheobuild 1000 was used. Concrete mix proportions, specific gravity and water absorption capacity of aggregates are given in Tables 2-4.

0.4 m thick specimens were employed more as pilot units to observe the crater formation, spalling and scabbing amount on a thinner specimen than as effective protection against the projectile used in the program.

CAC40 is a hydraulic binder i.e., a finely ground inorganic material. When mixed with water, it forms a paste that sets and hardens by means of hydration reactions and processes. After the hydration process has produced stable hydrates, it retains its strength and stability even under water. The main characteristic of CAC40 is that although its setting is quite slow in comparison with CEM I 42.5 R, its strength gain is very rapid. This feature is related to the oxide and compound composition of the cement. As the name implies, CAC40 is composed of mainly calcium aluminates and the main phase, mono calcium aluminate (CA), sets slowly but hardens very rapidly,

Table 2 Concrete mix proportions

	Group 1		Group 2	Group 3	Group 4
Compressive Strength, MPa	30	55	61	87	58
CEM I 42.5 R, kg/m^3	305	650	400	---	1400
CAC40, kg/m^3	---	---	---	550	---
Fly ash, kg/m^3	80	196	---	---	---
Silica fume, kg/m^3	---	---	30	30	50
Water, kg/m^3	177.7	223.7	170	200	450
Fine aggregate, kg/m^3	936	411	1091	404	---
Coarse aggregate, kg/m^3	848	744	730	1212	---
Normal plasticizer, kg/m^3	2.44	---	---	---	---
Hyper plasticizer, kg/m^3	---	16.9	5.2	5.5	---
Super plasticizer, kg/m^3	---	---	---	---	22
Steel fiber, kg/m^3	---	---	156	156	936

Table 3 Characteristics of aggregates used in Group 1

	0-4 mm	8-16 mm	16-22.4 mm
Unit weight	2.65	2.70	2.70
Water Absorption Capacity, %	1.65	0.55	0.48

Table 4 Characteristics of aggregates used in Groups 2 and 3

	0-4 mm	4-7 mm	7-15 mm
Unit weight	2.66	2.61	2.65
Water Absorption Capacity, %	1.22	2.20	0.80

liberating a large amount of heat of hydration (CEN/TC 51 N 802 2004, CEN/TC 51 N 645 2000, Neville 1975).

In the construction of HPSFRC specimens 156 kg/m^3 steel fibers were added into the concrete, equivalent to a ratio of 2 percent by volume. These low carbon fibers are cold drawn wire fibers, with hooked ends, and glued in bundles as shown in Fig. 1(a). This type of fibers has a minimum tensile strength of 1050 MPa. In SIFCON specimens, steel fibers with a minimum tensile strength of 1270 MPa at a volumetric ratio 12 percent were used. These fibers were also loose cold drawn wire fibers with hooked ends. Using glued steel fibers in the construction of HPSFRC specimens was a necessity because the fibers must first become loose in the concrete in order to avoid a lumpy texture. In SIFCON specimens, discrete fibers have been used to compose the slab using cement slurry. Other geometrical and mechanical properties of the fibers are given in Table 5 and Fig. 1(b).

Table 5 Physical and mechanical properties of fibers (Bekaert 2008)

Property	Fibers used in HPSFRC	Fibers used in SIFCON
Length, mm	60	30
Diameter, mm	0.75	0.62
Aspect Ratio	80	48
Coating	None	None
Tensile Strength, N/mm^2	1050	1270

<div style="text-align:center">(a)   (b)</div>

Fig. 1 Steel fibers (a) used in HPSFRC slabs (Dramix RC-80/60-BN), (b) used in SIFCON slabs (Dramix RL-45/30-BN) (Bekaert 2008)

2.2 Preparation of specimens

Cement, fly ash/silica fume, aggregates and steel fibers were first blended in dry condition. Later, water with plasticizer was gradually added to the mixture to provide a homogeneous mortar. The prepared mortar was poured into $2 \times 2 \times 0.6/0.4$ m wooden forms and vibrated. In the SIFCON specimens, steel fibers were placed into steel forms first. Then a ready-mix truck poured the slurry into the forms slowly. Two external vibrators accompanied the pouring process to fill the slurry homogeneously. Concrete samples were taken following standard procedures. The freshly poured concrete was cured under 20 ± 5°C temperature and 95% humidity for a week.
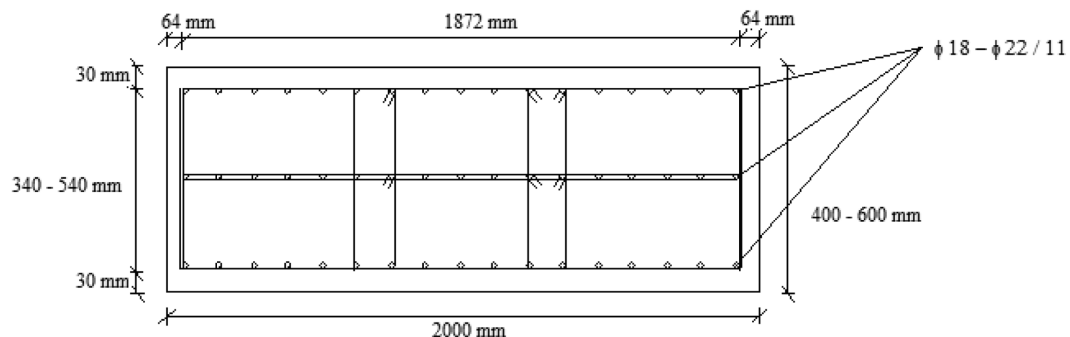

Fig. 2 Placement configuration of the reinforcement

In the program 2 m square reinforced concrete specimens 0.4 or 0.6 m thick were produced. Flexural bars 18 and 22 mm in diameter, and 10 mm diameter transverse bars were used. Flexural bars totaled 0.5 percent of the cross-sectional area in both directions. Configuration of reinforcement is shown in Fig. 2. The transverse reinforcement fulfilled the design requirements of shear walls in the Turkish Seismic Design Code (2007). The dimensions facilitated striking the target from a distance of one km.

2.3 Sample tests for mechanical properties of concrete and steel bars

Standard sample tests were performed to obtain the mechanical characteristics of materials in the production of specimens for use as input parameters in the numerical analyses. These characteristics involve strength, toughness and ductility measures for the concrete and the customary indices for the reinforcement. The field tests involved specimens being struck by a supersonic heavy caliber projectile that produced very high temperatures at the point of impact and hyper strain rates in the concrete. We did not have the means of conducting laboratory tests that would simulate these conditions. The values we report are thus a replication of customary concrete practice.

Standard compression and three-point bending tests were performed to obtain the compressive strength and flexural strength of the concrete. Standard cylindrical samples (150 mm × 300 mm)

Table 6 Results of three-point bending tests

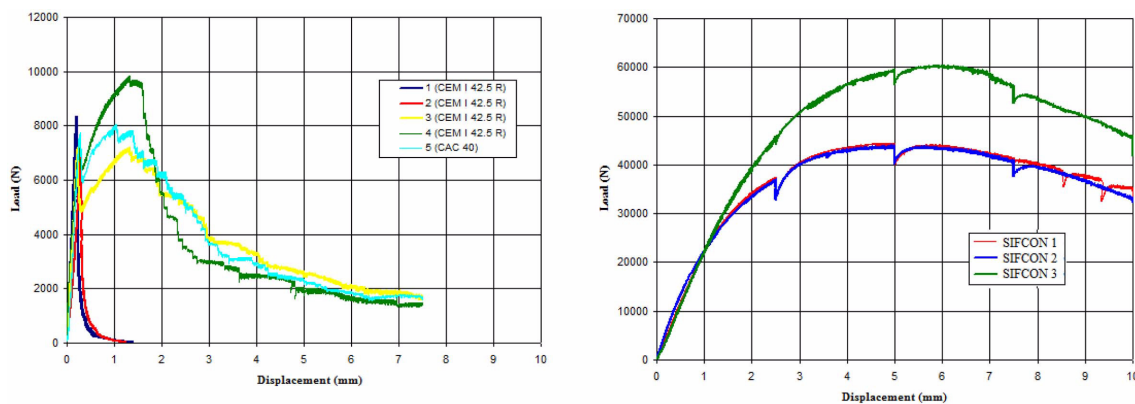| Specimen No.	Cement Type	Compressive Strength (MPa)	Average Flexural Strength (MPa)
1	CEM I 42.5 R	30	4.20
2	CEM I 42.5 R	55	4.60
3	CEM I 42.5 R	61	4.12
4	CEM I 42.5 R	61	5.77
5	CAC40	87	4.76
6	SIFCON	58	36.48
7	SIFCON	58	28.35
8	SIFCON	58	28.10

Fig. 3 Load-displacement curves obtained from three-point bending tests

Table 7 Results of steel bar tension tests

	Φ 10 mm	Φ 18 mm	Φ 22 mm
Yield strength, MPa	600.5	480.4	477.2
Tensile strength, MPa	702.3	608.3	664.9

were prepared. Characteristic strengths, the average of three cylinder tests are reported in Table 6 for each group of specimens.

Beam test specimens of $600 \times 150 \times 150$ mm were produced to perform three-point bending tests to obtain flexural strength of concrete. The results of these tests are given in Table 6 and Fig. 3. Thus material properties we report here are the customary quantities for standard engineering applications.

Steel bars used in the production of specimens were S420a quality described in the Turkish Standard for steel bars TS 708 (1996). They were subjected to tension tests to determine their tensile and yield strengths. The results of these tests are summarized in Table 7.

2.4 The projectile

Projectiles with the designation APFSDS-T (Armor Piercing Fin Stabilized Discarding Sabot – Tracer) of 105 mm diameter were employed in the experiments. This projectile has a tungsten core and an initial speed of over 4 Mach. Its mass is 5.57 kg. Technical specifications of the projectile are
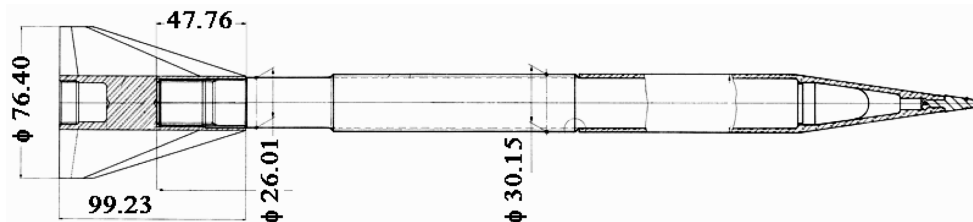

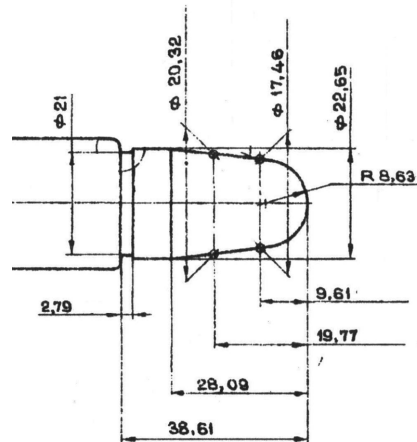Fig. 4 Sketch of 105 mm APFSDS-T in mm (MKEK 2010)

Fig. 5 Nose shape details of the projectile in mm (MKEK 2010)

Table 8 Technical specifications of 105 mm APFSDS-T projectile (MKEK 2010)

Gross mass (g)	Core mass (g)	Material	Total length (mm)	Initial velocity (m/s)	Range (m)
18000	5570	Tungsten	759	1485	4262

summarized in Table 8. Sketch and the nose shape details of the projectile are shown in Figs. 4 and 5.

2.5 Experimental set-up and measurements

Both impact velocity and residual velocity after perforation were measured by recording the shots by a high-speed camera capable of recording up to 250,000 frames per second under ideal conditions. The high-speed camera was placed on the same line of sight as the specimen and perpendicular to the shot line. Steel plates painted 10 cm-wide white and red stripes were located in the background at the front and rear sides of the specimens as speed gages. These plates allowed calculating the impact velocity and perforation from the video recordings. Craters that formed after the strike were measured and visual inspections were made of the global deformation of the specimens and type of perforation and scabbing. No other measurements were possible. The experimental set-up is shown schematically in Fig. 6.

3. Results of high-velocity impact experiments

In the experimental stage procedure, 13 specimens in four groups were fired at with the projectiles. In all groups, two separate shots were performed. Specimens 1-1, 2-1, 3-1 and 4-1 were targeted alone while other specimens were grouped together for the shots. The edge conditions of the slabs were "free-free" as they sat upon their bottom edges on the ground. Distance between the gun and the target was 800 m for Specimen 1-1, and 1000 m for all others.
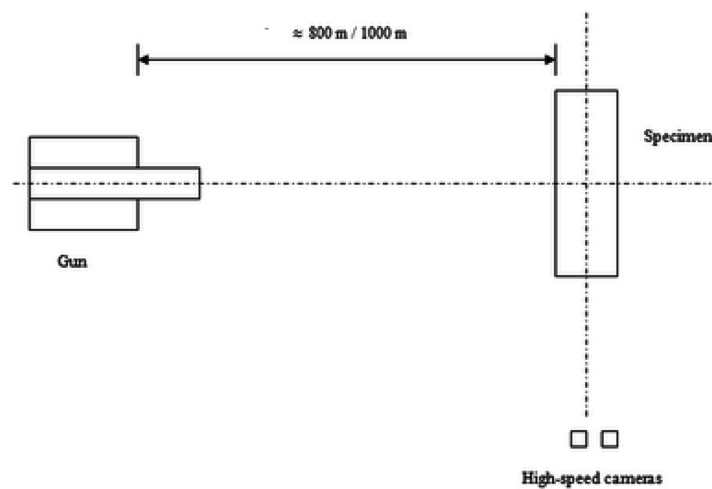

Fig. 6 Plan view of experimental set-up (not to scale)

Hitting the mark centrally was exacerbated by the paucity of the ammunition, so the gunner needed to fire trial shots before the main shots. Two such shots were fired at a dummy wooden testing board to calibrate the muzzle of the gun for wind, temperature and other ambient conditions.

Due to the supersonic velocity of the projectile, all shots caused thorough perforation of the target. Nevertheless, increase in the steel fiber quantity manifested an improved performance in reducing the deformation of the concrete specimens that could be verified at first sight. Measurements confirmed this observation.

The projectiles that penetrated the specimens could not be recovered after the experiments, but we have reason believe that there was no significant erosion in their physical properties because entry, through-travel and exit geometries of successively placed specimens were similar.

It should be noted that in the experiments, parts of concrete specimens subjected to projectile impact directly were wholly deformed, but because of intensive crowding of longitudinal and transverse bars, these parts looked as if they had been perforated only in the size of projectile. It follows that, concrete between the craters at the front and rear sides of specimens must be assumed as having failed fully. This observation was verified by our numerical simulations of the experiments that are presented in the accompanying article.

3.1 Observations of damage on specimens

3.1.1 Group 1

In this group the specimens were conventionally reinforced concrete slabs. In the first test, Specimen 1-1 was the lone target, and proved to offer little protection against the projectile that struck it as it perforated it. During the next test, Specimens 1-2, 1-3 and 1-4 were placed in succession at 2-m spacing. Both tests resulted in complete perforation of the targets. Crater dimensions were measured at both sides of specimens.

The test of Specimen 1-1 was recorded by high-speed camera with very poor resolution due to poor visibility. Therefore, impact and post-perforation velocities could not be calculated accurately from the film.

Specimens before and after impact are shown in Figs. 7 and 8. Measured deformation, impact velocity and perforation values are summarized in Tables 9 and 10, respectively. Even with three specimens placed in the path of the bullet its exit velocity from the final slab was still supersonic.
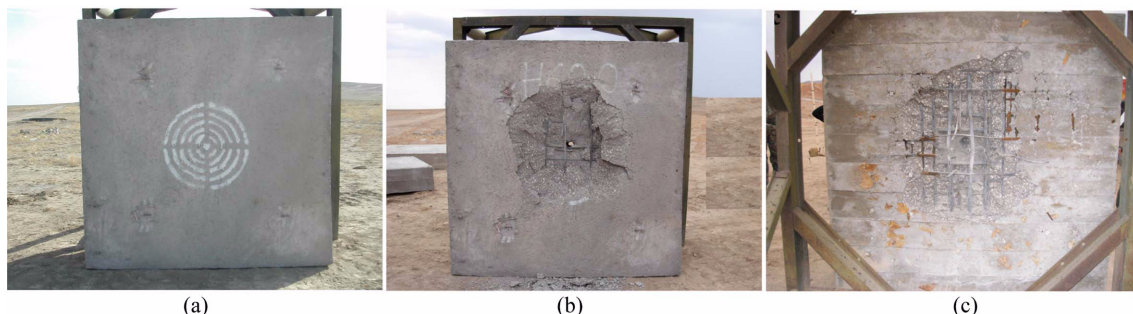

(a)   (b)   (c)

Fig. 7 Specimen 1-1 before and after impact, (a) front side before impact, (b) front side after impact, (c) rear side after impact
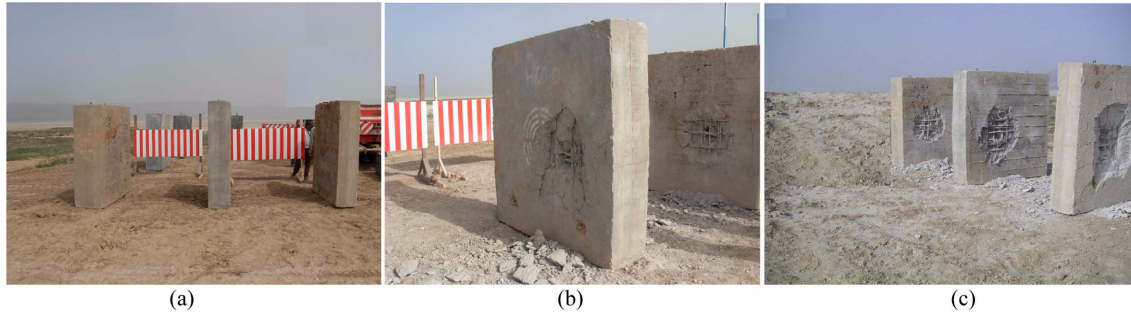
Fig. 8 Specimens 1-2, 1-3 and 1-4 before and after impact, (a) specimens before impact, (b) front sides after impact, (c) rear sides after impact

Table 9 Deformations measured in Group 1

No.	Front Face			Rear Face		
	Crater Diameter (mm)		Max. Depth of Crater (mm)	Crater Diameter (mm)		Max. Depth of Crater (mm)
	Horizontal	Vertical		Horizontal	Vertical	
1-1	980	1030	160	640	1010	80
1-2	630	690	140	860	840	130
1-3	840	900	150	1080	950	170
1-4	910	790	130	1040	980	180

Table 10 Impact velocity and perforation values in Group 1

No.	Impact Velocity (m/s)	Perforation (m/s)	Reduction of Velocity Caused by Impact (percent)
1-1	Unreliable recording	Unreliable recording	---
1-2	1437	1333	7.24
1-3	1333	1143	14.25
1-4	1143	430	62.40

Crater areas at the entry and exit locations remained large, reflecting the brittle character of normal concrete. Deformations near the centers of specimens were small due to the restraining capability of steel bars in tension. The initial impact velocity on Specimen 1-2 was larger than on the two specimens that stood behind it, but the crater area that formed in this specimen was smaller. It is judged that the principal reason for this was the 0.6 m thickness. The 0.4 m thick Specimens (1-3 and 1-4) had larger crater dimensions.

Although the high-speed camera recordings showed that the projectile impacted the specimens in perpendicular fashion, when the holes on the destroyed specimens were investigated, it was observed that there might have been a small deviation angle of trajectory. For this reason, calculations reflecting change in velocity for the situations of normal and oblique impact will be given in Part II.

3.1.2 Group 2

In this group, specimens containing the same amount of reinforcement as Group 1 in addition to 2 percent steel fibers were tested. Specimen 2-1 was targeted alone while Specimens 2-2 and 2-3 were placed in series. Tests that resulted in complete perforation were recorded by the high-speed camera except for Specimen 2-1 due to instrument malfunction. Specimens before and after impact are shown in Figs. 9 and 10. Measured deformation, impact velocity and perforation values are given in Tables 11 and 12.

Fig. 9 Specimen 2-1 after impact, (a) front side, (b) close-up view of front side, (c) rear side, (d) close-up view of rear side

Table 11 Deformations measured in Group 2

No.	Front Face			Rear Face		
	Crater Diameter (mm)		Max. Depth of Crater (mm)	Crater Diameter (mm)		Max. Depth of Crater (mm)
	Horizontal	Vertical		Horizontal	Vertical	
2-1	550	540	90	590	820	130
2-2	530	440	70	810	670	130
2-3	640	650	90	750	940	160

Table 12 Impact velocity and perforation values in Group 2

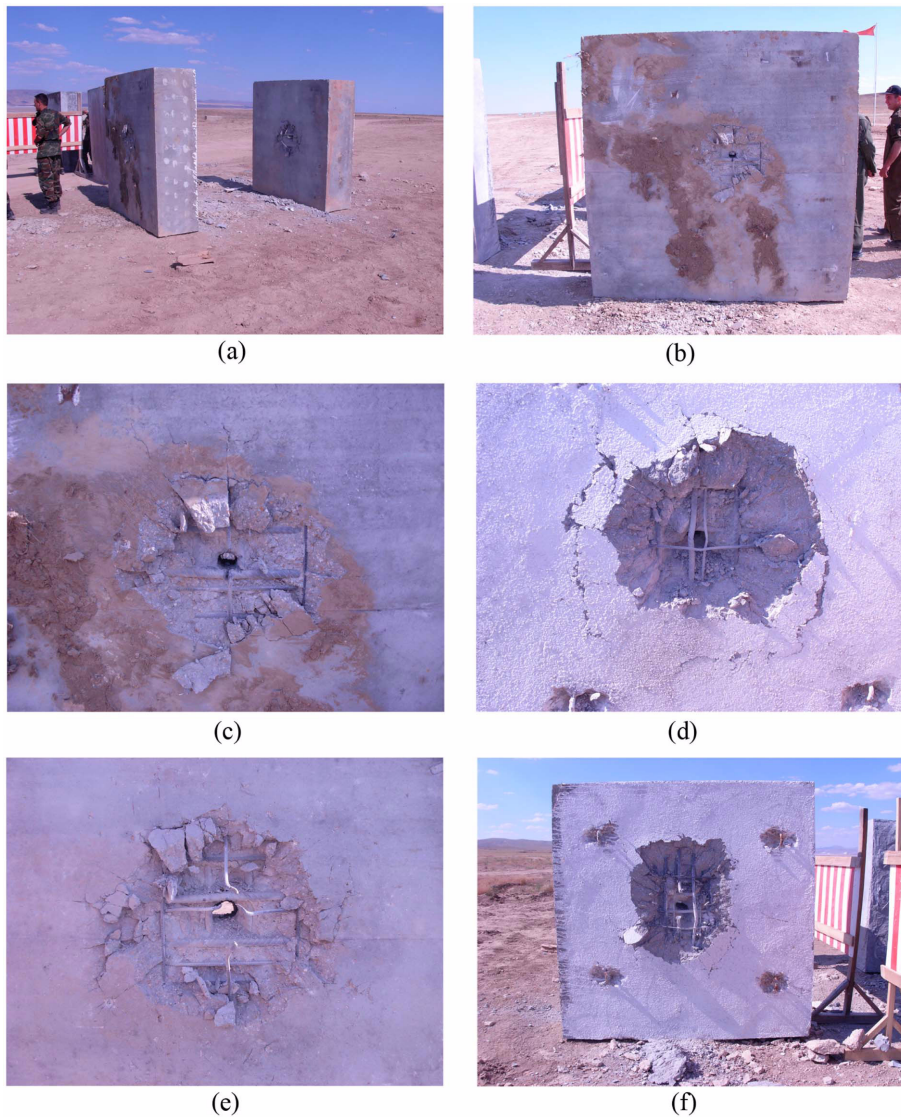| No.	Impact Velocity (m/s)	Perforation (m/s)	Reduction of Velocity Caused by Impact (percent)
2-1	Unreliable recording	Unreliable recording	---
2-2	1450	1281	11.66
2-3	1281	1014	20.84

Fig. 10 Specimens 2-2 and 2-3 after impact, (a) general view, (b) front side of Specimen 2-2, (c) close-up view of front side of Specimen 2-2, (d) close-up view of rear side of Specimen 2-2, (e) close-up view of front side of Specimen 2-3, (f) rear side of Specimen 2-3

The principal reason of smaller crater dimensions in specimens in Group 2 than those in Group 1 was steel fiber reinforcement. The effects of steel fibers were also observed in the differences of spalling and scabbing in the second group of specimens as compared with the first group of specimens where only regular steel bars had been provided as reinforcement. This comparison was a clear demonstration of the positive effect of steel fibers for reducing deformation. Compressive strength of concrete in Group 2 was not significantly higher than strength in Group 1 (61 vs. 55 MPa). It is thus not convincing to state that higher compressive strength led to a reduced deformation. The reason of the occurrence of greater crater depth and over-scabbing on the rear sides of Specimens 2-2 and 2-3 was identified as the inadvertently thick cover concrete in the forms leading to weak cover. This situation can be observed in Figs. 10(d) and (f).

In nearly all impact events, the bullet struck either the flexural or the transverse bars. Inspections showed that it had cut the bars if contact had been normal and central. If the impact had been eccentric, it had bent the bars which it had contacted. In some specimens, due to the wave propagation along the steel bars the local vibration caused by projectile impact, slightly larger crater dimensions and increased amount of spalling and scabbing at entry and exit sides had resulted. This behavior may be seen in Figs. 10(c) and (e) as concrete particles around the crater perimeter.

3.1.3 Group 3

Specimens produced with CAC40 with reinforcement mesh and 2 percent of steel fibers by volume were subjected to firing tests. Unfortunately, none of these tests could be captured by the camera due to instrumentation problems. Still, the deformations caused by the projectile impact on the specimens were measured. Similar to Group 2 Specimen 3-1 was shot at alone. Specimens 3-2 and 3-3 were placed in tandem. All were 0.6 m thick.

The specimens after impact are shown in Figs. 11 and 12. Measured deformation, impact velocity and perforation values are given in Tables 13 and 14. A notable observation could be made on the rear sides of Specimens 3-1, 3-2 and 3-3. Their behavior could be described as "over-scabbing" compared to the front face.

Specimens in Group 2 and Group 3 contained the same amount of steel fibers (2 percent), but different types of cement, CEM I 42.5 R and CAC40, respectively. Their concrete compressive strengths were 61 MPa and 87 MPa, respectively. It is believed that the smaller crater dimensions in Group 3 compared with those in Group 2 occurred due to the higher compressive strength of concrete, but not because of the cement type. Also comparing the deformation size of these specimens with those in Group 1, the contribution of steel fibers in preventing larger deformation

Table 13 Deformations measured in Group 3

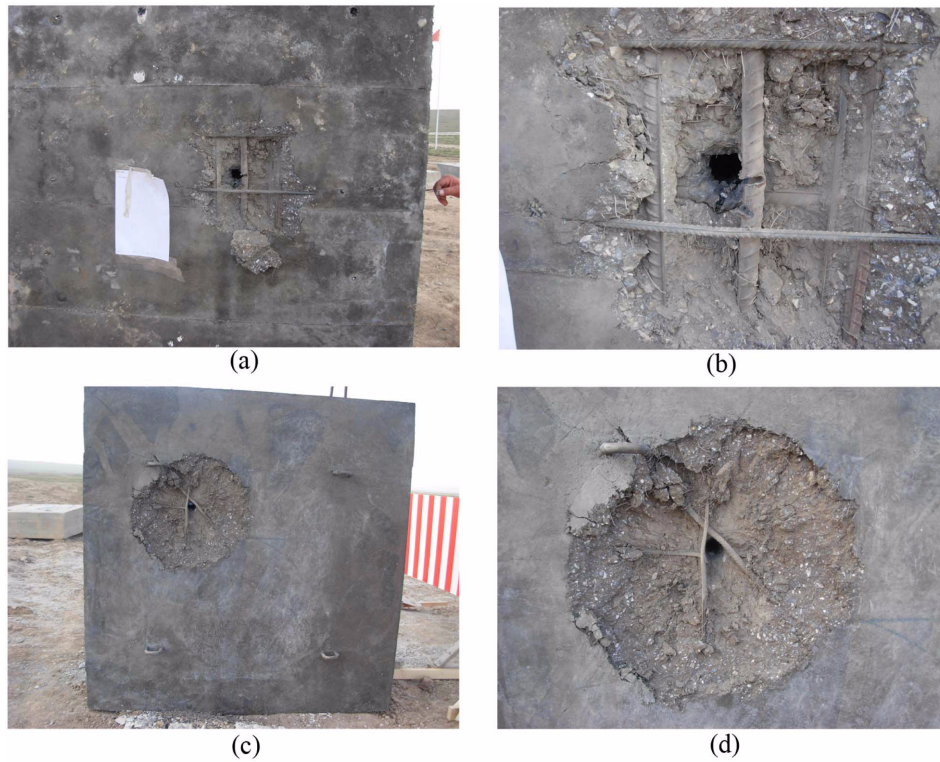| No.	Front Face			Rear Face		
	Crater Diameter (mm)		Max. Depth of Crater (mm)	Crater Diameter (mm)		Max. Depth of Crater (mm)
	Horizontal	Vertical		Horizontal	Vertical	
3-1	410	390	60	720	670	100
3-2	250	330	90	570	680	100
3-3	510	740	180	730	750	130

Fig. 11 Specimen 3-1 after impact, (a) front side, (b) close-up view of front side, (c) rear side, (d) close-up
view of rear side

Table 14 Impact velocity and perforation values in Group 3

No.	Impact Velocity (m/s)	Perforation (m/s)	Reduction of Velocity Caused by Impact (percent)
3-1	Unreliable recording	Unreliable recording	---
3-2	Unreliable recording	Unreliable recording	---
3-3	Unreliable recording	Unreliable recording	---

could be clearly observed. Because of the dense reinforcement placed inside the specimens, projectile struck the steel bars in all specimens and this led to a significant reduction of velocity.

3.1.4 Group 4

In the fourth group, specimens produced by cement slurry and 12 percent of steel fibers were tested. Specimen 4-1 was targeted alone while Specimens 4-2 and 4-3 were placed in series. These tests resulted in complete perforation and were captured by the camera. Deformations on the targets were measured on both sides.

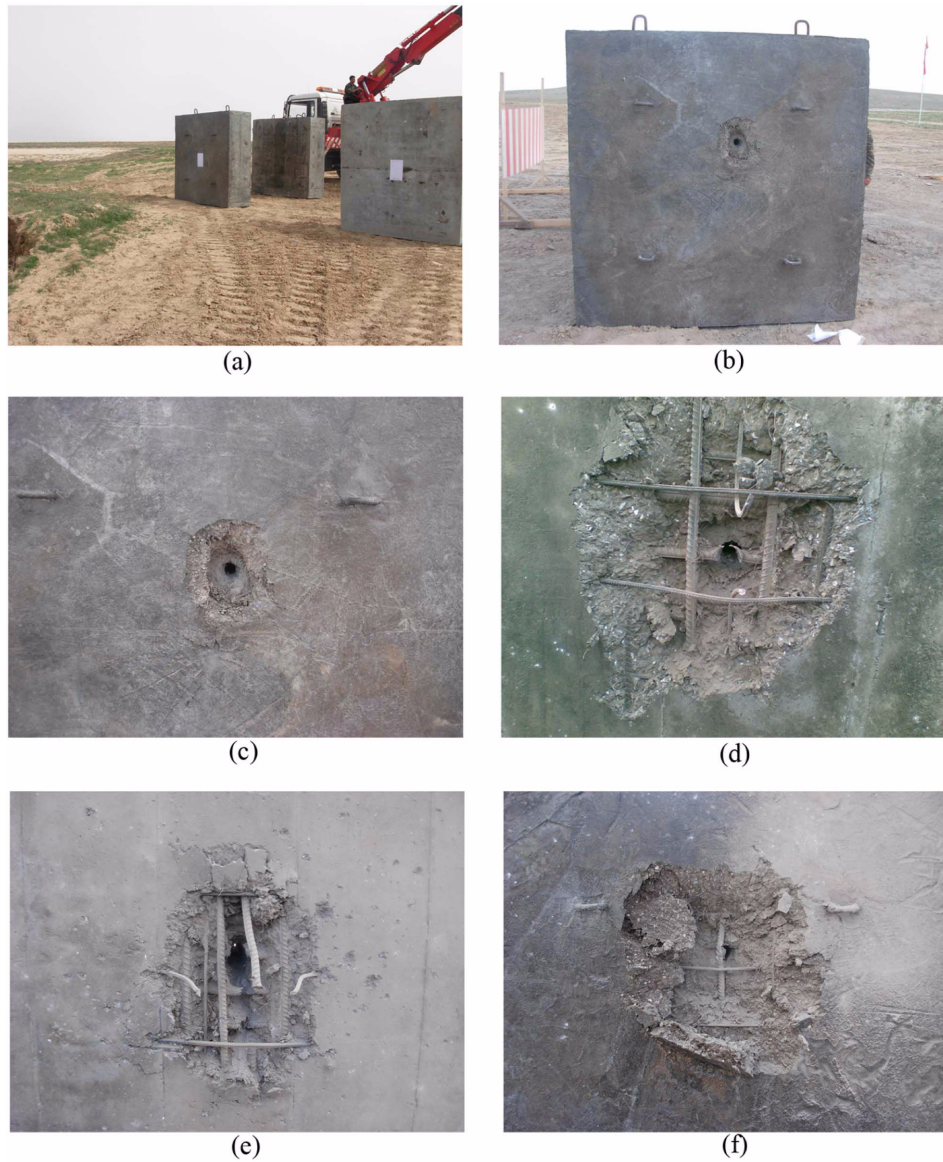Pictures from high-speed camera recordings of the shot performed for Specimens 4-2 and 4-3 are

Fig. 12 Specimen 3-2 and 3-3 after impact, (a) general view, (b) front side of Specimen 3-2, (c) close-up view of front side of specimen 3-2, (d) close-up view of rear side of Specimen 3-2, (e) close-up view of front side of Specimen 3-3, (f) close-up view of rear side of Specimen 3-3

given in Fig. 13. Specimens before and after impact are shown in Figs. 14 and 15. Measured deformation, impact velocity and perforation values are given in Tables 15 and 16. The heavy damage on the rear side of Specimen 4-1 was attributed to the poorly compacted and segregated concrete layer at the bottom of the form at the time of casting.

High amount of steel fibers that the SIFCON specimens contained leads to limit the crater area to the smallest. The significance of tensile and shear strengths and toughness of concrete in impact
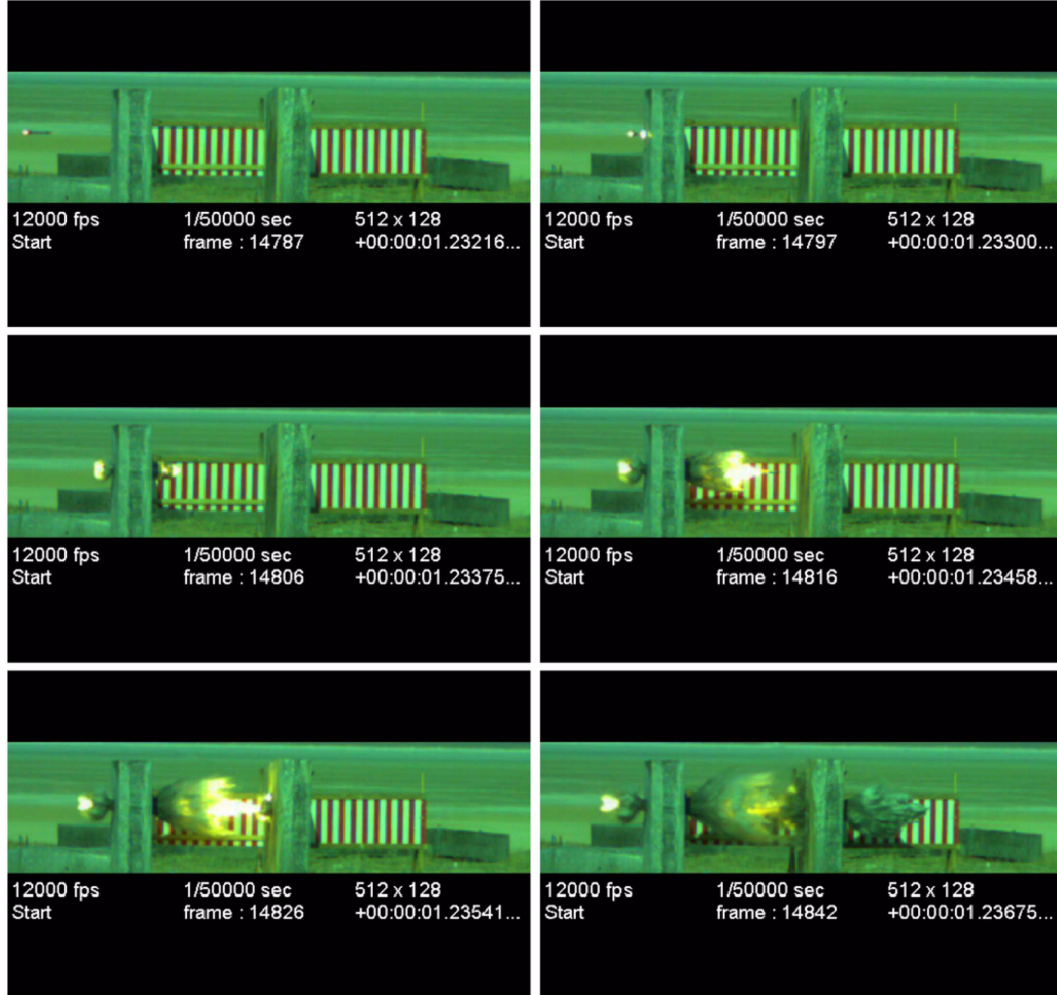
Fig. 13 Pictures from high-speed camera recording of the shot performed for Specimens 4-2 and 4-3

phenomena was observed clearly. Investigating the reduction of velocity ratios, it can also be seen that they behaved well, but not better than specimens containing steel bars.

The deformation that occurred at the front side of Specimen 4-3 shown in Fig. 15(e) was caused by concrete lumps that tore away from the rear side of Specimen 4-2 during scabbing. These pieces hit Specimen 4-3 and punched its front side as the projectile bore through it.

The same holds for Specimen 4-1 which displayed near total disintegration on its rear side. In this case over-scabbing led to complete loss of the integrity of the specimen. The cause of this apparent over-destruction was judged again to be the misplaced concrete in the forms to levels where steel fibers had segregated during placement, creating in effect a weak crustal layer. It was observed that the crust concrete had started to crack before the firing experiments due to the lack of steel fibers. This phenomenon is visible in Figs. 14(c) and 15(d) and (f). That a protective concrete wall that contains only steel fibers for reinforcement is not a desirable option for design seems to be a natural corollary of the evidence.
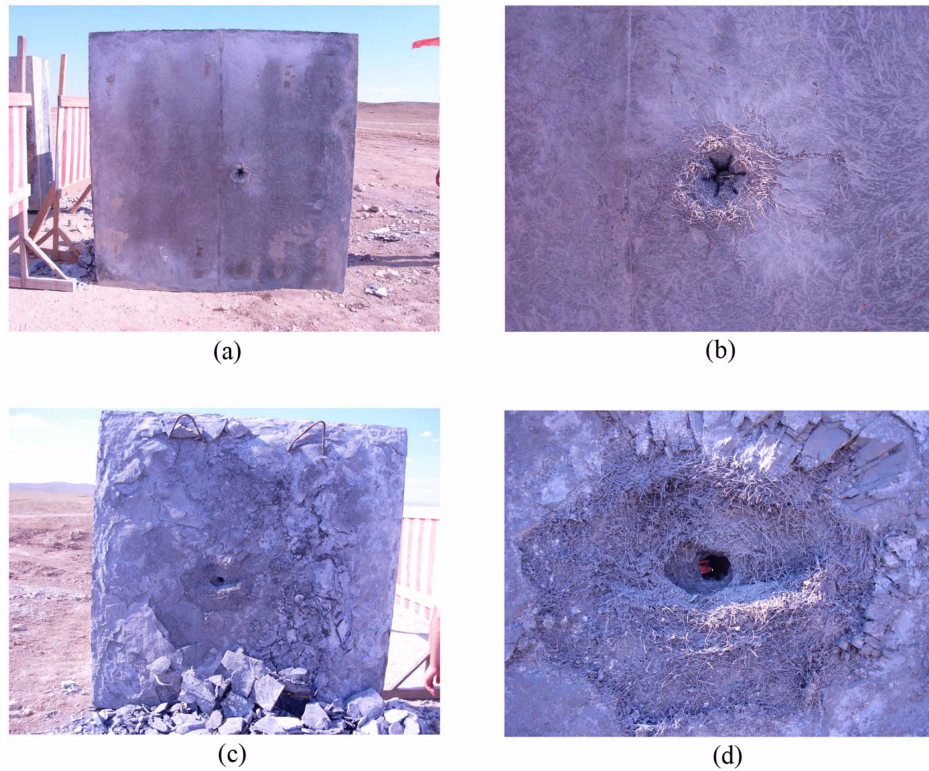
Fig.14 Specimen 4-1 after impact, (a) front side, (b) close-up view of front side, (c) rear side, (d) close-up view of rear side

Table 15 Deformations measured in Group Four

No.	Front Face			Rear Face		
	Crater Diameter (mm)		Max. Depth of Crater (mm)	Crater Diameter (mm)		Max. Depth of Crater (mm)
	Horizontal	Vertical		Horizontal	Vertical	
4-1	150	160	40	490	540	80
4-2	150	170	40	460	480	110
4-3	160	220	50	720	650	140

Table 16 Impact velocity and perforation values in Group Four

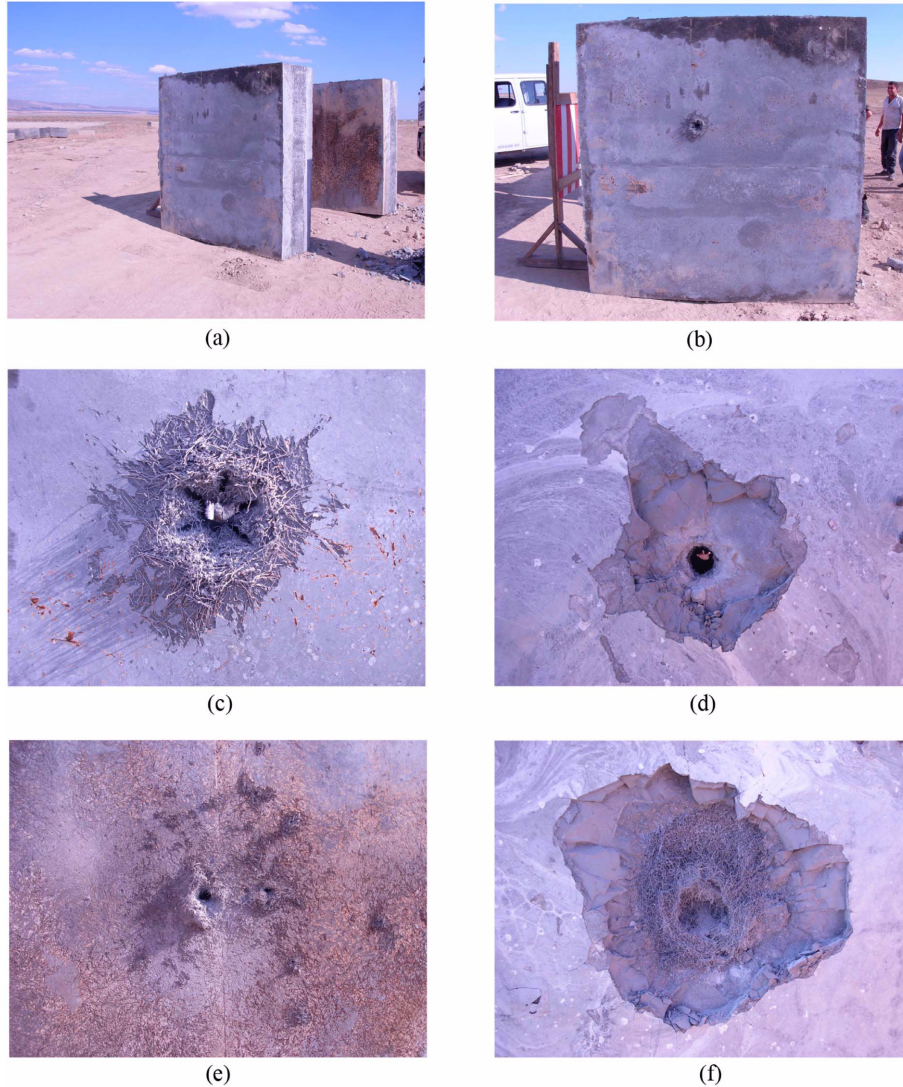| No.	Impact Velocity (m/s)	Perforation (m/s)	Reduction of Velocity Caused by Impact (percent)
4-1	1461	1275	12.73
4-2	1450	1325	8.62
4-3	1325	1145	13.58

Fig. 15 Specimens 4-2 and 4-3 after impact, (a) general view, (b) front side of Specimen 4-2, (c) close-up view of front side of Specimen 4-2, (d) close-up view of rear side of Specimen 4-2, (e) close-up view of front side of Specimen 4-3, (f) close-up view of rear side of Specimen 4-3

4. Conclusions

In the experimental phase of this study, 2×2 m slabs with either 0.4 m or 0.6 m thickness including both conventional reinforcement and steel fibers or only steel fibers were targeted by projectiles fired with a muzzle velocity of over 4 Mach. The shots resulted in complete perforation even when the target specimens were arranged so that they stood in series in close proximity to one another. Impact and post-perforation velocities of Specimens 1-2, 1-3, 1-4, 2-2, 2-3, 4-1, 4-2 and 4-3 were measured as planned using high-speed cameras. These measurements for other specimens

could not be recorded due to various technical or human problems and poor visibility conditions. Perforation, scabbing, shape of missile path and crater sizes were carefully measured on all specimens.

In the experimental part of the study that is described in this article, patterns of deformation for the specimens were observed and supplementary material tests were performed. These results provided the input for the numerical simulations that will be described in Part II of this article.

An immediate general statement is that traditionally placed dense reinforcement showed better performance in reducing the velocity due to direct impact. The results also clearly showed that steel fibers enable a good performance in decreasing the area of the crater and volume of scabbing and spalling if they are used in addition to reinforcement. Their performance in reducing the exit velocity of the projectile was fair.

In general, higher concrete compressive strength led to smaller crater dimensions. No findings could be obtained about the effect of CAC-40 cement due to poor camera recordings. The better performance of CAC-40 specimens compared with those consisting of CEM I 42.5 R cement were attributed to the higher concrete strength.

A significant observation was based on the rear sides of Specimens 4-1, 4-2 and 4-3 where the integrity of the specimen was compromised and substantial loss of concrete occurred upon exit of the projectile. The reason of the occurrence of this apparent over destruction was the crust of weak concrete on the top side of the specimen where steel fibers had segregated during placement. In fact it was observed that concrete had started to fracture and delaminate even before the bullet impact test had been carried out due to the scarcity of steel fibers in the crust. A good view of this behavior can be seen in Fig. 14(c). The same cause leading to greater crater depth in rear sides of Specimens 2-2 and 2-3 was also the flaw in manufacturing the specimens resulting in a weak layer of concrete over the reinforcement cage.

The crater dimensions on the front sides of the specimens where the projectile first impacted such as 2-2, 3-2 and 4-2 were smaller than the dimensions on the front side of the secondary specimens of the group, 2-3, 3-3 and 4-3. The main reason of this situation was that, the front sides of the
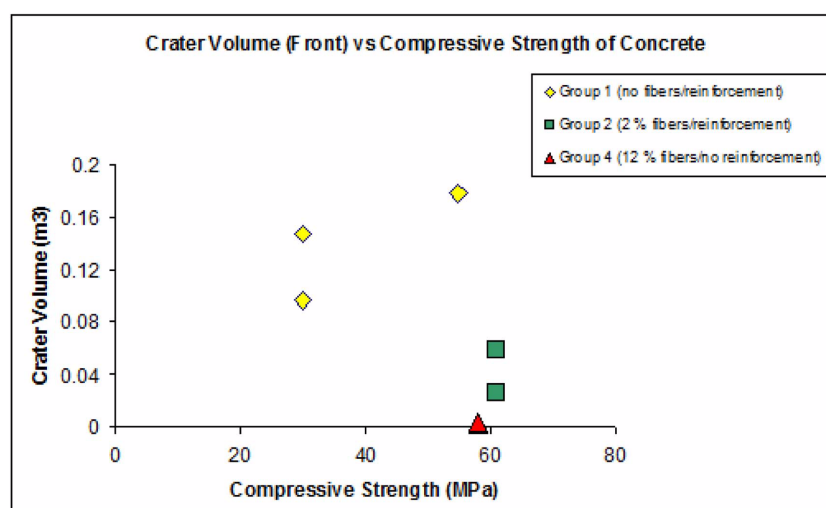

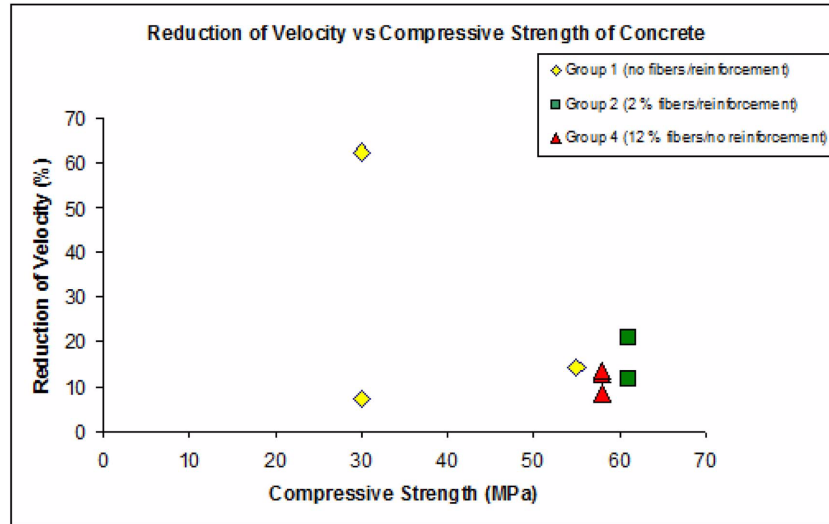Fig. 16 Crater volume (Front) vs. compressive strength of concrete

Fig. 17 Reduction of velocity vs. compressive strength of concrete
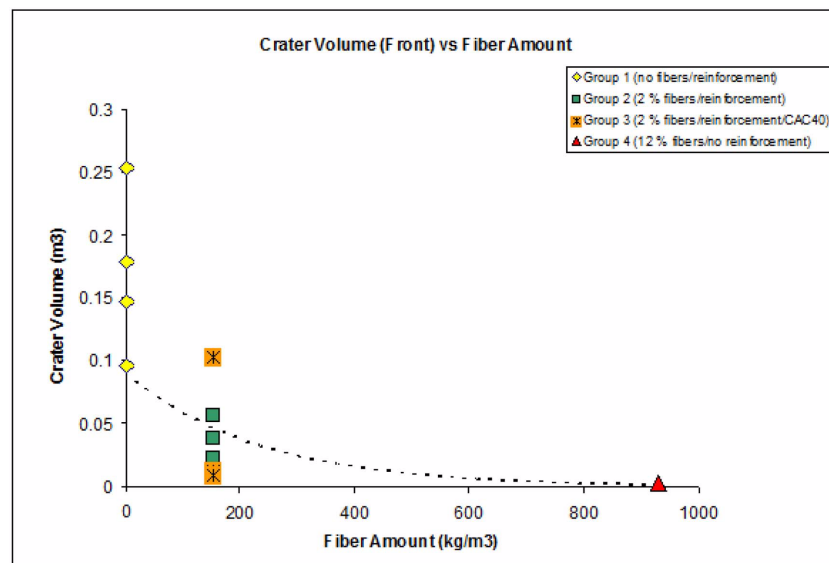

Fig. 18 Crater volume (Front Side) vs. fiber amount

secondary specimens were also subjected to particle impact caused by scabbing of the primary ones.

In Figs. 16-19, we present several measures damage in the specimens as a function of material properties. Fig. 16 show that the compressive strength of concrete has a positive effect on limiting the deformation on the specimens.

The effect of compressive strength of concrete on reducing projectile velocity is more tenuous (Fig. 17). Other parameters such as reinforcement amount and type must be taken into account before reaching a better defined conclusion.

Figs. 18 and 19 show the effect of steel fiber amount on the crater size. Higher fiber amount
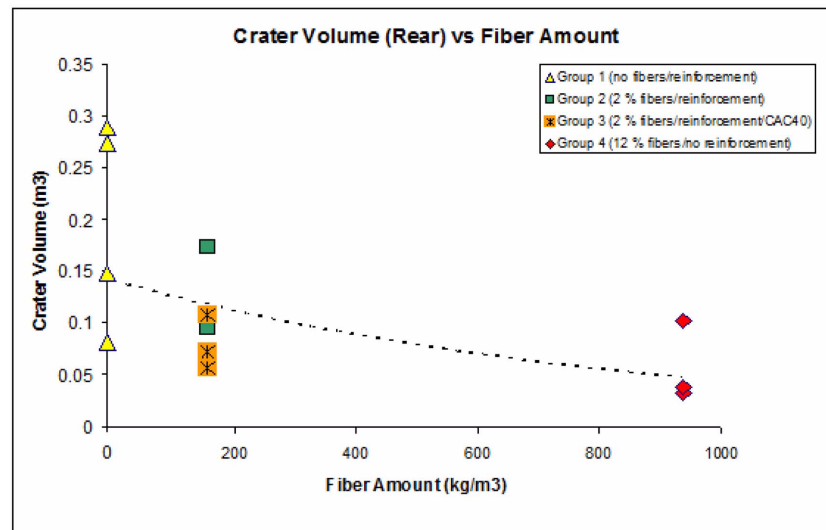
Fig. 19 Crater volume (Rear Side) vs. fiber amount

limits the deformation increasing the tensile strength of concrete. Spalling and scabbing were also minimized by the positive effects of steel fibers. The dotted lines in these diagrams are indicative of the general trend that needs to be established by additional tests.

Acknowledgments

Disclaimer

The commercial products named in this article are intended only for description of the experimental environment and do not necessarily imply their endorsement or approval by the authors or any other party.

References

ABAQUS Users' Manual (2007), Version 6.7, Simulia, Dassault Systemes, Providence, Rhode Island.
Bekaert (2008), Product Data Sheets of RC-80/60-BN and RL-45/30-BN, www.bekaert.com.
Beppu, M., Miwa, K., Itoh, M., Katayama, M. and Ohno, T. (2008), "Damage evaluation of concrete plates by high-velocity impact", *Int. J. Impact Eng.*, **35**(12), 1419-1426.
CEN/TC 51 N 645 (2000), Calcium Aluminate Cement. Report of CEN/TC 51 WG 6 TG1, Krakow, Poland.
CEN/TC 51 N 802 (2004), prEN 14647 Calcium Aluminate Cement: Composition, Specifications and Conformity Criteria, Lisbon, Portugal.

ConWep User's Guide (1993), Applications of TM 5-855-1, Fundamentals of Protective Design for Conventional Weapons, Department of the Army, Waterway Experiment Station, Corps of Engineers, Vicksburg, Mississippi.

Dancygier, A.N. (2009), "Characteristics of high performance reinforced concrete barriers that resist non-deforming projectile impact", *Struct. Eng. Mech.,* **32**(5), 685-699.

Luo X., Sun W., and Chan S.Y.N. (2000), "Characteristics of high-performance steel fiber-reinforced concrete subject to high velocity impact", *Cement Concrete Res.,* **30**(6), 907-914.

MKEK (2010), Turkish Mechanical and Chemical Industry Corporation, http://www.mkek.gov.tr/ foUrunDetaylari. aspx?iKodUrun=273&iKodUrunKategorisi=120, March.

Neville, A. (1975), *High Alumina Cement Concrete*, John Wiley & Sons, New York.

Orphal, D.L., Franzen, R.R., Charters, A.C., Menna, T.L. and Piekutowski, A.J. (1997), "Penetration of confined boron carbide targets by tungsten long rods at impact velocities from 1.5 to 5.0 km/s", *Int. J. Impact Eng.,* **19**(1), 15-29.

Özşahin, E. and Tolun, S. (2010), "Influence of surface coating on ballistic performance of aluminum plates subjected to high velocity impact loads", *Mater. Design,* **31**(3), 1276-1283.

PS3D Theory Manual and Verification Examples (2005), Numerics GmbH, Petershausen, Germany.

Puente, J.L., Varas, D., Loya, J.A. and Zaera, R. (2009), "Analytical modeling of high velocity impacts of cylindrical projectiles on carbon/epoxy laminates", *Compos. Part A-Appls.,* **40**(8), 1223-1230.

Quek, S.T., Lin, V.W.J. and Maalej, M. (2010), "Development of functionally-graded cementitious panel against high-velocity small projectile impact", *Int. J. Impact Eng.,* **37**(8), 928-941.

Teng, T.L., Chu, Y.A., Chang, F.A., Shen, B.C. and Cheng, A.S. (2008), "Development and validation of numerical model of steel fiber reinforced concrete for high-velocity impact", *Comp. Mater. Sci.,* **42**(1), 90-99.

TM 5-855-1 (1998), Technical Manual-Design and Analysis of Hardened Structures to Conventional Weapons Effects, The Departments of Army, Air Force and Navy and the Defense Special Special Weapons Agency, Washington, D.C.

TS 708 (1996), *Steel Bars for Concrete*, Turkish Standards Institution, Ankara, Turkey.

Turkish Seismic Design Code (2007), Deprem Bölgelerinde Yapılacak Binalar Hakkında Yönetmelik, Bayındırlık ve İskân Bakanlığı, Ankara.

Vossoughi, F., Ostertag, P.O., Monterio, P.J.M. and Johnson, G.C. (2007), "Resistance of concrete protected by fabric to projectile impact", *Cement Concrete Res.,* **37**(1), 96-106.

Zhang, M.H., Shim, V.P.W., Lu, G. and Chew, C.W. (2005), "Resistance of high-strength concrete to projectile impact", *Int. J. Impact Eng.,* **31**(7), 825-841.

Zhang, Q., Wang, X., Huang, F., Chen, L. and Guo, X. (2009), "An experimental and numerical study of the dynamic response of a free-free aluminum beam under high velocity transverse impact", *Int. J. Impact Eng.,* **36**(12), 1385-1393.

Zukas, J.A., Nicholas, T., Swift, H.F., Greszczuk, L.B. and Curran, D.R. (1992), *Impact Dynamics*, Krieger Publishing Company, Malabar, FL.